

ANL/MSD/CP--90867  
CONF-960401--70

**STRAIN, STRUCTURE AND ELECTRONIC STATES IN  
MBE GROWN (Nb,Ti)O<sub>2</sub> MIXED RUTILE\***

S.A. Chambers<sup>1</sup>, Y. Gao<sup>1</sup>, S. Thevuthasan<sup>1</sup>, S. Wen<sup>2</sup>,  
K.L. Merkle<sup>2</sup>, N. Shivaparan<sup>3</sup>, and R.J. Smith<sup>3</sup>

<sup>1</sup>Environmental Molecular Sciences Laboratory  
Pacific Northwest National Laboratory  
Richland, Washington

<sup>2</sup>Materials Science Division  
Argonne National Laboratory  
Argonne, IL 60439

<sup>3</sup>Department of Physics  
Montana State University  
Bozeman, Montana

August 1996

The submitted manuscript has been created by the University of Chicago as Operator of Argonne National Laboratory ("Argonne") under Contract No. W-31-109-ENG-38 with the U.S. Department of Energy. The U.S. Government retains for itself, and others acting on its behalf, a paid-up, nonexclusive, irrevocable worldwide license in said article to reproduce, prepare derivative works, distribute copies to the public, and perform publicly and display publicly, by or on behalf of the Government.

RECEIVED

SEP 03 1996

OSTI

To be presented at the Materials Research Society 1996 Spring Meeting,  
San Francisco, CA, April 8-12, 1996.

\*Work supported by the U.S. Department of Energy, Basic Energy Sciences-Materials Sciences, under contracts DE-AC06-76RLO 1830 (PNNL) and #W-31-109-ENG-38. The ion channeling analysis at Montana State University was supported in part by NSF Grant DEM 9409205.

DISTRIBUTION OF THIS DOCUMENT IS UNLIMITED

MASTER

ng

**DISCLAIMER**

**Portions of this document may be illegible  
in electronic image products. Images are  
produced from the best available original  
document.**

# STRAIN, STRUCTURE AND ELECTRONIC STATES IN MBE GROWN (Nb,Ti)O<sub>2</sub> MIXED RUTILE

S.A. CHAMBERS<sup>1</sup>, Y. GAO<sup>1</sup>, S. THEVUTHASANI<sup>1</sup>, S. WEN<sup>2</sup>, K.L. MERKLE<sup>2</sup>, N. SHIVAPARAN<sup>3</sup>, and R.J. SMITH<sup>3</sup>

1- Environmental Molecular Sciences Laboratory, Pacific Northwest National Laboratory, Richland, Washington. 2 - Materials Science Division, Argonne National Laboratory, Argonne, Illinois. 3 - Department of Physics, Montana State University, Bozeman, Montana.

## ABSTRACT

We have grown and characterized epitaxial Nb<sub>x</sub>Ti<sub>1-x</sub>O<sub>2</sub> on TiO<sub>2</sub>(110) and (100) for the purpose of investigating the role of chemically-inequivalent metal atoms on the thermal and photocatalytic properties of TiO<sub>2</sub>. Our goal is to introduce, in a highly controlled fashion, a Group VA transition metal into the lattice of a Group IVA transition metal oxide without altering the crystallographic structure. So doing would alter the electronic structure in interesting and potentially useful ways by the addition of one valence electron per substituted metal atom. However, strain builds in the film as more Nb is added at a rate which depends on the crystallographic orientation of the growth direction. Films grown along (110) can accommodate Nb mole fractions as high as ~0.3 without forming misfit dislocations, whereas those grown along (100) are limited to ~10 at. % Nb. Nb-O bond lengths in Nb<sub>x</sub>Ti<sub>1-x</sub>O<sub>2</sub> are the same as Ti-O bond lengths in pure TiO<sub>2</sub> prior to the onset of dislocation formation. The extra 4d valence electron per Nb atom forms a nonbonding band which is degenerate with bonding states in the valence band region.

## INTRODUCTION

TiO<sub>2</sub> is a very effective photocatalyst for the destruction of chlorinated organics [1]. Electron-hole pair production by UV light absorption coupled with low recombination velocities allows the electron and the hole to promote reduction and oxidation, respectively, of species sorbed on the surface of the particle. There are reports in the literature that the addition of a few atomic percent of Nb<sub>2</sub>O<sub>5</sub> to TiO<sub>2</sub> powder significantly increases the extent of photocatalytic destruction of dichlorobenzene when using 5.5 eV UV light as an excitation source [2]. However, the enhancement mechanism is unknown. It is difficult to extract mechanistic information from studies of powders because each particle exposes several crystal faces, and neither the surface structure nor composition are unique or well characterized. In order to perform definitive studies on such systems, it is helpful to prepare well-defined, single-crystal surfaces which enable detailed investigations of the geometric and electronic structure to be carried out. Then, the observed surface thermal- and photochemistry of the material can be correlated with the properties of the surface. Molecular beam epitaxy is a desirable way to make such surfaces in that one can maintain control over the film composition, structure and morphology by varying the relative fluxes, growth rates, and diffusion rates across the surface. In this paper, we describe such an investigation for mixed (Nb,Ti)O<sub>2</sub> rutile films. We describe the growth and detailed characterization of the geometric and electronic structure of these materials.

## EXPERIMENTAL

All MBE growth and *in-situ* measurements were carried out in a system described elsewhere [3]. *Ex-situ* high-resolution transmission electron microscopy (TEM) measurements were carried out using a JEOL 4000 EX2 microscope. Polished TiO<sub>2</sub> rutile single crystals oriented to within ± 1° of (110) were used as substrates. The substrates were ultrasonically cleaned in acetone and methanol prior to insertion into the MBE chamber. Once under ultrahigh vacuum (UHV), substrates were initially rid of carbon by electron beam heating at 600°C for 10 minutes while being exposed to activated oxygen from an electron cyclotron resonance (ECR) plasma source at

an oxygen partial pressure of about  $4 \times 10^{-5}$  torr and a plasma power of 200W. However, after this treatment, the  $\text{TiO}_2$  surfaces were found to contain trace amounts of Ba and Mg impurities as measured by x-ray photoelectron spectroscopy (XPS). Thus, a number of cycles of argon-ion sputtering and annealing in activated oxygen at  $600^\circ\text{C}$  were carried out until no impurities were detected. The sputtering and annealing treatment resulted in stoichiometric surfaces as shown by sharp Ti 2p peaks with no indication of  $\text{Ti}^{3+}$  by XPS.  $\text{Ti}^{3+}$  reveals the presence of oxygen vacancies, which leaves behind electrons that partially reduce nearest-neighbor  $\text{Ti}^{4+}$  cations in the lattice. In addition, the surface was well ordered after this treatment, as judged by the quality of  $1 \times 1$  reflection high-energy electron diffraction (RHEED) and low-energy electron diffraction (LEED) patterns.

$\text{Nb}_x\text{Ti}_{1-x}\text{O}_2$  films were grown by coevaporating Ti and Nb in an overpressure of activated oxygen from the ECR plasma source at a substrate temperature of  $600^\circ\text{C}$  [4-6]. Several films were grown on a single substrate with increasing Nb mole fraction in each successive film. Typical growth rates were 0.3-0.4 monolayer (ML) per second, and the oxygen partial pressure in the growth chamber during growth was typically  $3-5 \times 10^{-5}$  torr with the ECR plasma source running at 200 watts. These settings constitute oxygen-rich growth conditions, and result in atomically flat and stoichiometric  $\text{Nb}_x\text{Ti}_{1-x}\text{O}_2$  surfaces. Structure was monitored during growth by RHEED. The relative fluxes measured from two water-cooled quartz crystal oscillators revealed Nb concentrations ranging from a few to  $\sim 40$  at.%. After growth, the  $\text{Nb}_x\text{Ti}_{1-x}\text{O}_2$  films were transferred into the analytical chamber and characterized *in situ* by LEED, XPS, and scanned-angle x-ray photoelectron diffraction (XPD). One specimen was removed from the MBE chamber and prepared for high-resolution TEM lattice imaging.

## RESULTS

### *Film Structure*

$\text{Nb}_x\text{Ti}_{1-x}\text{O}_2$  epitaxial films grow as single-domain single crystals for all compositions investigated, although misfit dislocations nucleate at higher values of  $x$ . We show in figures 1 and 2 representative LEED patterns for growth on  $\text{TiO}_2(110)$  and  $(100)$  substrates, respectively. Patterns marked as  $x=0$  are for pure  $\text{TiO}_2$  buffer layers grown by homoepitaxy. A  $(3 \times 1)$  reconstruction, brought about by microfacetting, is visible in the pattern for the  $(100)$ -oriented substrate [7-11]. This pattern arises from annealing in ultrahigh vacuum at temperatures in excess of  $\sim 600^\circ\text{C}$ . Surface reduction occurs through oxygen loss in this temperature range, and is accompanied by the formation of stable  $(110)$  microfacets. The surface reverts to a  $(1 \times 1)$  structure upon annealing in the oxygen plasma, and after growth of  $\text{TiO}_2$  buffer layers and mixed  $(\text{Nb}/\text{Ti})\text{O}_2$  films under oxygen rich conditions [6]. Sharp, bright patterns with very low background reveal that surfaces with excellent long-range order and smooth morphologies grow up to  $x = \sim 0.3$  and  $\sim 0.1$  for growth along  $(110)$  and  $(100)$ , respectively. Above these mole fractions, high background develops, indicating the formation of point defects, and transmission patterns emerge in the RHEED (not shown), revealing significant roughening of the surfaces. It is at these Nb concentrations that the strain energies in the films exceed the energies required to nucleate misfit dislocations. This transition can be clearly seen in high-resolution TEM lattice images. One such image is shown in figure 3, which shows the interface of  $\text{Nb}_{0.28}\text{Ti}_{0.72}\text{O}_2$  and  $\text{Nb}_{0.43}\text{Ti}_{0.57}\text{O}_2$ , both grown on a  $(110)$ -oriented substrate. The primary beam was oriented along  $[111]$ , and the bright spots at the corners of each parallelogram are rows of Nb and Ti cations. Oxygen rows are not visible because of the weak scattering strength of oxygen anions. Dislocations begin to appear after the growth of several monolayers of  $\text{Nb}_{0.43}\text{Ti}_{0.57}\text{O}_2$ . Although point defects are not visible in TEM lattice images due to a lack of long-range order, the appearance of high background in the RHEED and LEED patterns at mole fractions in excess of  $\sim 0.3$  on  $(110)$ -oriented substrates reveals that such defects are generated along with the misfit dislocations.

Interestingly, there is no measurable change in metal-oxygen bond lengths surrounding Nb cations when Nb substitutes for Ti in the lattice. We have performed scanned-angle XPD at

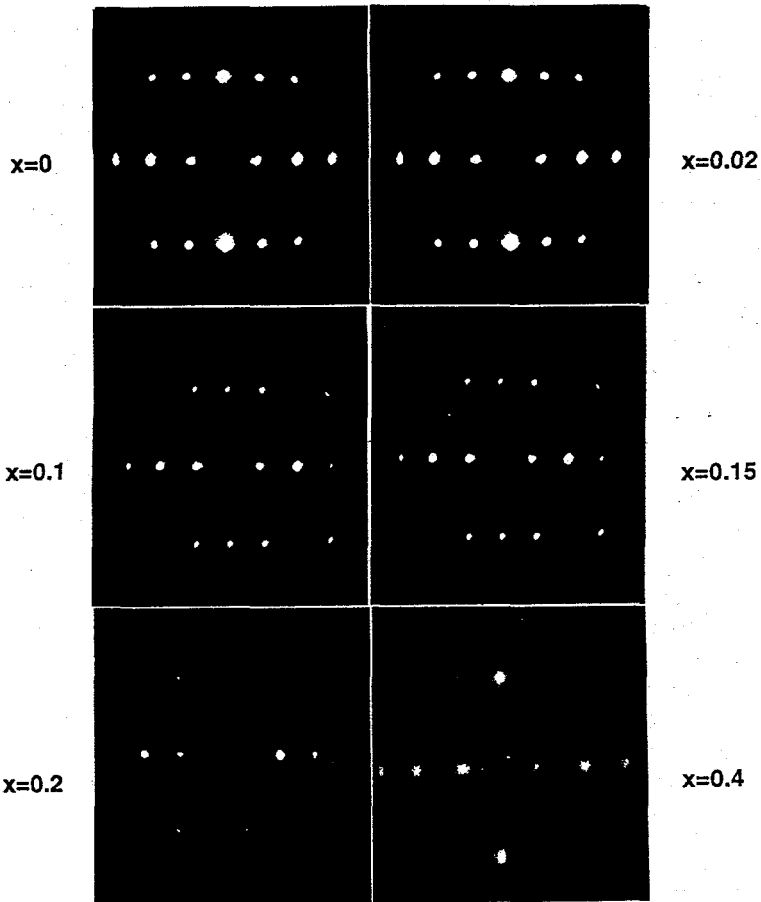


Fig. 1 LEED patterns obtained at 120 eV for  $Nb_xTi_{1-x}O_2$  epitaxial films on  $TiO_2(110)$  substrates as a function of  $x$ .

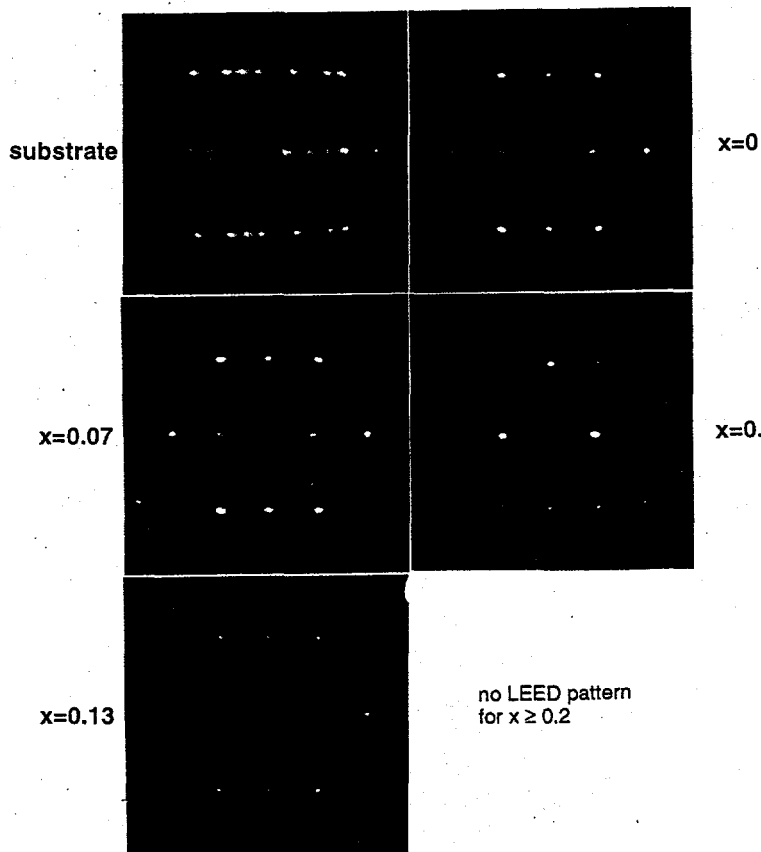


Fig. 2 LEED patterns obtained at 110 eV for  $Nb_xTi_{1-x}O_2$  epitaxial films on  $TiO_2(100)$  substrates as a function of  $x$ .

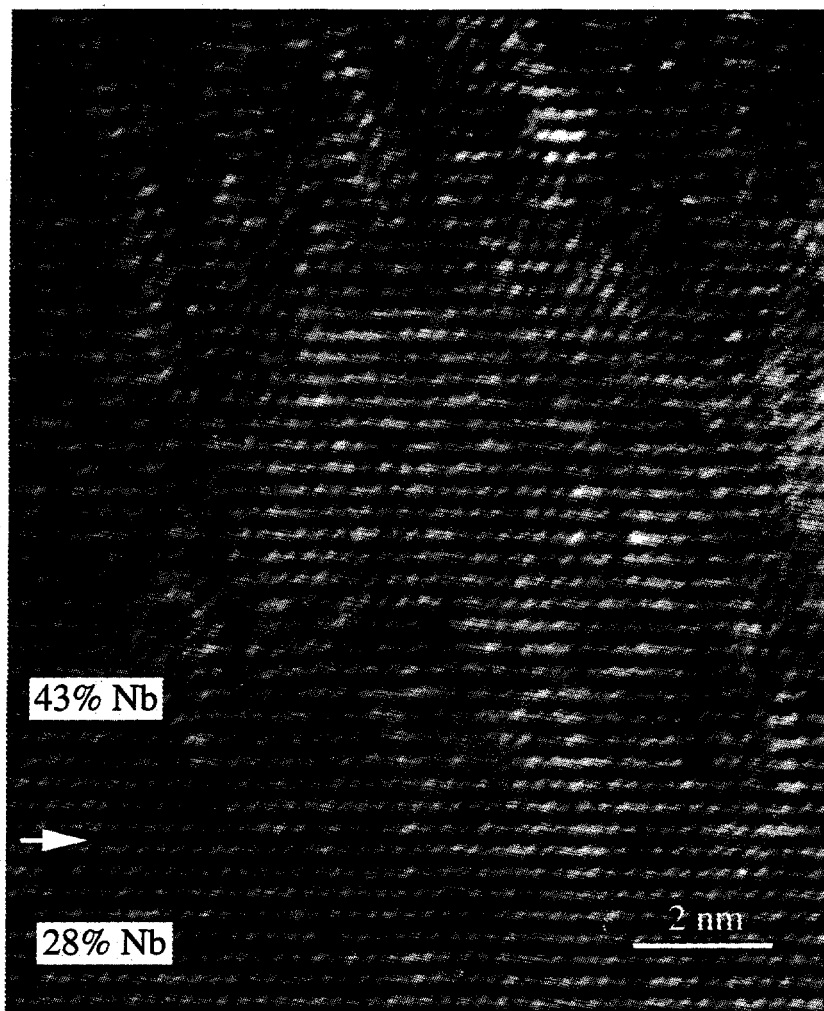


Fig. 3 High-resolution TEM lattice image viewed along  $[111]$  of the interface of epitaxial films of  $\text{Nb}_{0.28}\text{Ti}_{0.72}\text{O}_2$  and  $\text{Nb}_{0.43}\text{Ti}_{0.57}\text{O}_2$  grown on  $\text{TiO}_2(110)$ .

high angular resolution and ion channeling experiments on (110) and (100) oriented films, respectively. Analysis of these data reveal that the Nb-O bond lengths in  $\text{Nb}_x\text{Ti}_{1-x}\text{O}_2$  are within  $0.1\text{\AA}$  of Ti-O bond lengths in  $\text{TiO}_2$  for  $x$  less than the critical value for misfit dislocation generation. The axial Nb-O bond length in  $\text{NbO}_2$  rutile is 12% larger than the Ti-O axial bond length in  $\text{TiO}_2$ . The equatorial bond lengths are within 1% in the two oxides [12, 13]. Thus, the Nb-O bond length may elongate in order to relieve the interatomic repulsion resulting from Nb substituting in the smaller  $\text{TiO}_2$  lattice. In order to do so, however, the adjacent O-Ti equatorial bond length would have to compress, which would result in considerable interatomic repulsion in that bond. This situation is denoted in the crystal diagram seen on the right side of figure 4. Also shown in figure 4 are angular distributions of Ti 2p and Nb 3p<sub>3/2</sub> photoemission obtained at an angular acceptance of  $\pm 1^\circ$  for several polar angles relative to the surface for a 5 at. % Nb-doped (110)-oriented film. The diffraction modulation is a sensitive function of the local structural environment of the emitting atom [14]. In the dilute limit ( $< \sim 10\%$ ), the modulation of Ti 2p photoemission will be identical to that observed in pure  $\text{TiO}_2$ . This result comes about because the diffraction modulation originates in scattering events within a few near neighbor shells of the emitter. In all likelihood, these shells will not contain any Nb for a given Ti emitter if  $x = 0.05$ . The Nb 3p<sub>3/2</sub> diffraction modulation is essentially the same as that seen in the Ti 2p scan. This result reveals that there are negligible differences in the local structural environments surrounding the two kinds of atoms. This conclusion is corroborated by comparison of Nb 3p<sub>3/2</sub> scans with those calculated with multiple scattering theory in which we assume: (i) no change in axial and equatorial bond length compared those found in  $\text{TiO}_2$ , and (ii) a  $0.1\text{\AA}$  expansion in the axial bond length surrounding substitutional Nb. These two calculated scans (not shown) are virtually the same, and agree reasonably well with experiment, suggesting that at least to within  $0.1\text{\AA}$ , there is no change in bond length upon substituting Nb for Ti [15]. This result is further

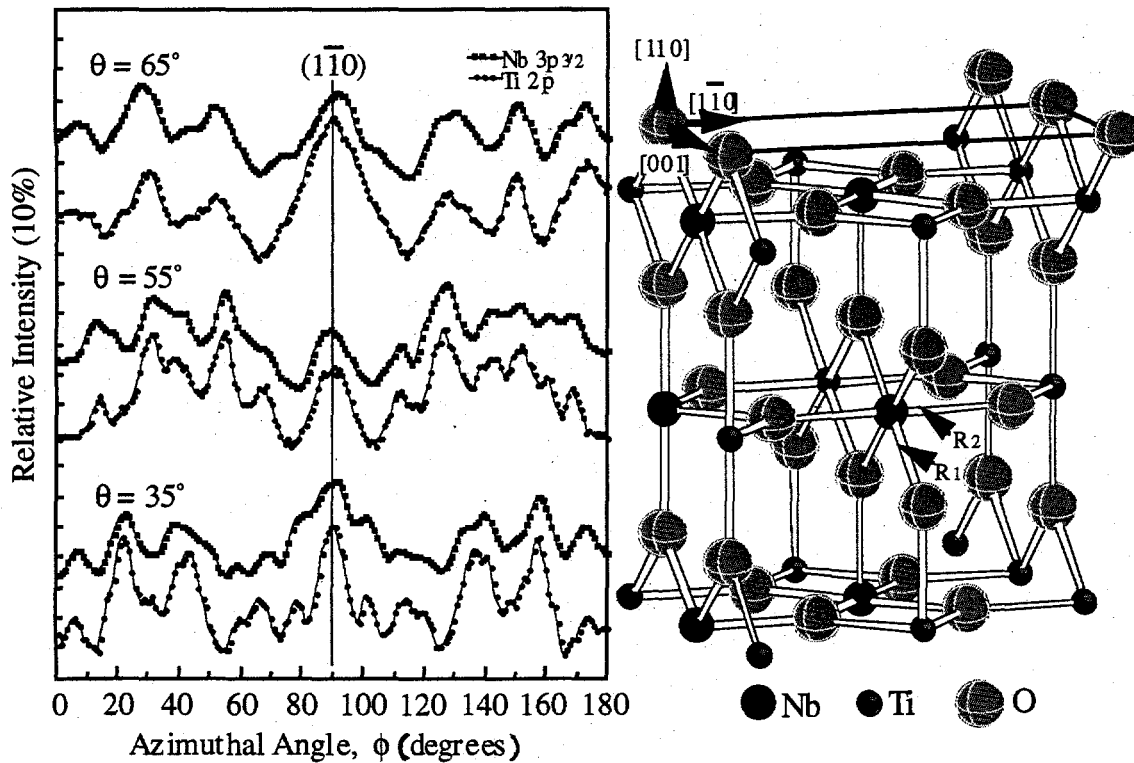


Fig. 4 Ti 2p and Nb  $3p_{3/2}$  angular distributions for epitaxial  $\text{Nb}_{0.05}\text{Ti}_{0.95}\text{O}_2$  on  $\text{TiO}_2(110)$ .

corroborated by ion channeling rocking curves for (100)-oriented  $\text{Nb}_{0.10}\text{Ti}_{0.90}\text{O}_2$ , which are shown in figure 5. These scans show very narrow ( $\sim 1.3^\circ$ ) angular widths for both Ti and Nb backscattering when the incident He beam is oriented along (100). Although we have not yet performed a detailed quantitative analysis of these results and the associated minimum yield data, it appears that to within  $\sim 0.1\text{\AA}$ , there is no displacement of substitutional Nb from bulk cation lattice positions [16].

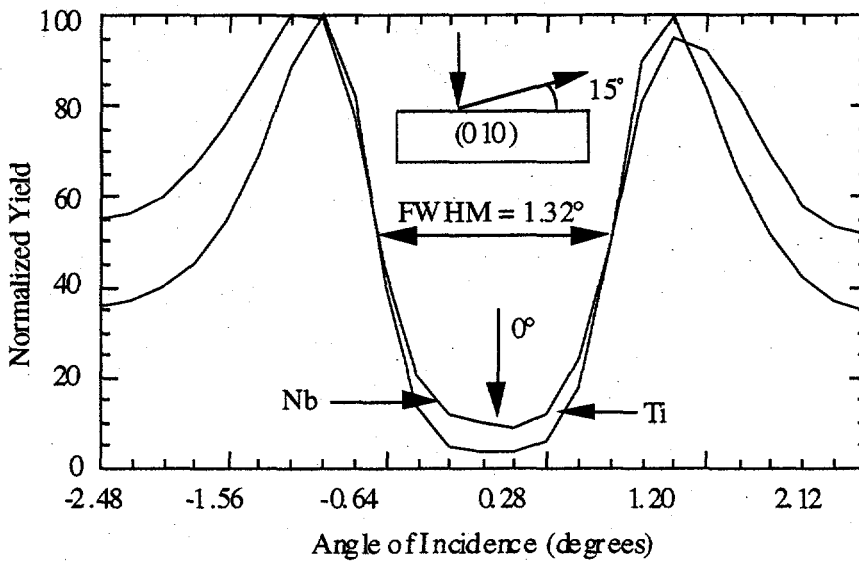


Fig. 5 Ion channeling rocking curves for epitaxial  $\text{Nb}_{0.10}\text{Ti}_{0.90}\text{O}_2$  on  $\text{TiO}_2(100)$ .

## Surface Enhancement of Nb

Although Nb substitutes for Ti at lattice sites and does not form secondary phases, there is compelling evidence that Nb segregates to lattice sites in the near-surface region, rather than distributing equally throughout the film. XPS Ti 2p and Nb 3p<sub>3/2</sub> core-level intensities obtained at normal emission ( $\theta=90^\circ$ ) and at shallow-angle emission ( $\theta=35^\circ$ ) suggest near-surface segregation of Nb. For instance, XPS derived values of  $x$  for a (110)-oriented film determined to be  $\sim 20$  Nb at. % by the QCO are 0.25 and 0.35 for  $\theta=90^\circ$  and  $35^\circ$ , respectively. To further quantify this result, we have used ion channeling results to determine the extent of near-surface Nb enhancement. This analysis is summarized in figure 6 for a nominally 10 Nb at. % film grown on TiO<sub>2</sub>(100). We have extracted the number of Nb cations per unit area as a function of depth from the channeling and backscattering spectra. The unit of area consists of a slab of twelve unit cells, as shown in fig. 6. There are twenty four cations lattice sites per slab. The analysis reveals that seven of these cation sites are occupied by Nb in the top slab, compared to three in the second slab and only one in the third (and deeper) slab. Thus, the surface-layer composition is Nb<sub>0.3</sub>Ti<sub>0.7</sub>O<sub>2</sub>, whereas the bulk composition is Nb<sub>0.04</sub>Ti<sub>0.96</sub>O<sub>2</sub> [16]. This result has interesting implications for the effect of substitutional Nb on the surface chemistry of this material.

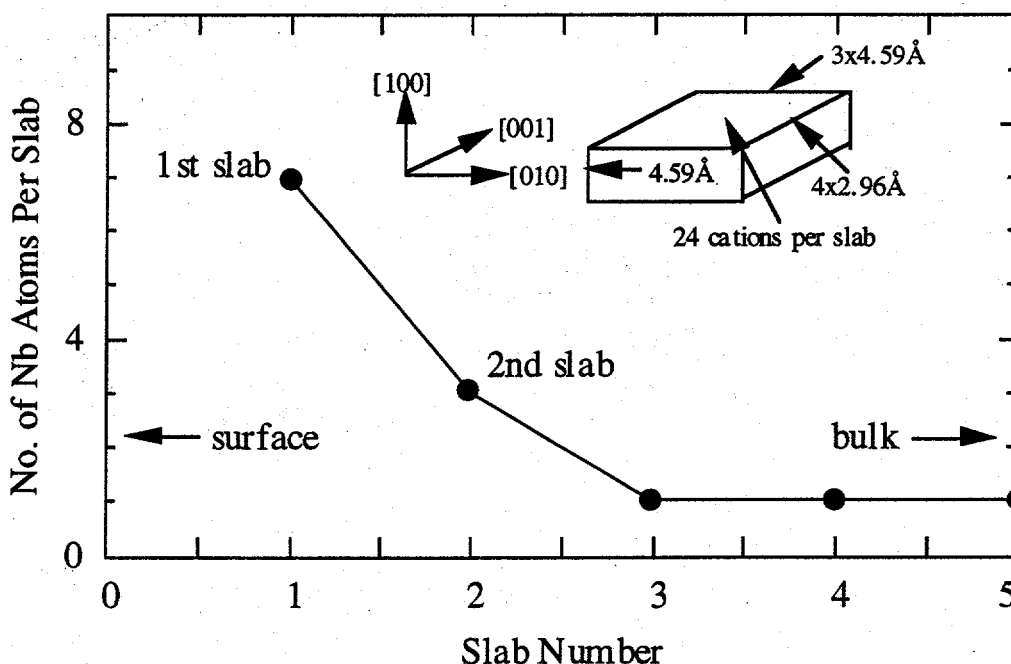


Fig. 6 Composition as a function of depth for epitaxial Nb<sub>0.10</sub>Ti<sub>0.90</sub>O<sub>2</sub> on TiO<sub>2</sub>(100) based on ion scattering experiments.

### Strain Accumulation and Relief

The amount of strain which accumulates in the film as a function of Nb mole fraction ( $x$ ) is readily calculated using elastic theory. The calculation is particularly simple for growth along (110). In this case, the strain is biaxial, and one of the strain axes is [110], the growth direction. Strain in this direction is readily taken up by the free surface. Thus, the strain is actually uniaxial. We can estimate the strain energy along  $[1\bar{1}0]$  in the plane of the surface by recognizing that each O-Nb-O bond pair surrounding a substitutional Nb cations is stressed by an amount ( $\Delta y$ ) equal to  $2(2.23-1.98\text{\AA}) = 0.52\text{\AA}$  in the  $[1\bar{1}0]$  direction. This stress can be thought of as being distributed over some amount of length along  $[1\bar{1}0]$  which decreases with increasing  $x$ . In the limit of a 1 at. % Nb film, this distance ( $y$ ) is equal to  $50R_1 + 50R_2$ , where  $R_1$  and  $R_2$  are the equatorial and axial bond lengths in rutile, respectively. For some general Nb mole fraction  $x$ ,  $y$  is given by  $(50R_1 + 50R_2)/100x$ . The elastic energy is then readily calculated using

Hooke's law by integrating the stress-strain product in the  $[\bar{1}10]$  direction. The result is  $E_{el} = (1/2)Y_y \epsilon_y^2$ , where  $Y_y$  is Young's modulus and  $\epsilon_y = (dy/y)$ , as given above. In doing this calculation, we have used Young's modulus for polycrystalline  $TiO_2$  since the crystallographic dependence of  $Y_y$  is not known for  $TiO_2$ . The elastic energy is then estimated to be  $E_{el} = 9.9x^2$  (GPa), and is equal to 0.89 GPa at  $x=0.30$ , the point at which dislocations form during growth along the (110) direction.

The factor-of-three difference in the amount of Nb that can be accommodated in (110)- and (100)-oriented films before relaxation occurs is a result of anisotropic strain. As mentioned above, the axial bond length,  $R_2$ , increases by 12% in going from  $TiO_2$  to  $NbO_2$ , whereas the equatorial bond length,  $R_1$ , increases by only 1% [12, 13]. Thus, the amount of in-plane stress in each film depends on the orientations of  $R_1$  and  $R_2$  with respect to the growth plane. In  $(Nb,Ti)O_2(110)$ , alternating rows of cations have  $R_2$  lying entirely in the growth plane;  $R_2$  is oriented along the growth direction in the other rows. In contrast, *every* cation row has a component of  $R_2$  in the growth plane in  $(Nb,Ti)O_2(100)$ . Thus, only half the cations are subjected to in-plane stress when the growth plane is (110) whereas all cations are experience in-plane stress when growing along (100). These geometries are shown in figure 7. As a result of this anisotropic lattice strain, we expect that more Nb can be accommodated during growth along (110) than along (100). In principle, the in-plane stress would be negligible up to  $x=0.5$  if all the incident Nb accumulated in the unstrained rows on the (110) growth front. However, we expect a statistical distribution of Nb in both strained and unstrained rows on (110), so that film strain would build and relaxation would presumably occur at mole fractions less than 0.5 along (110), which is consistent with our observations [5].

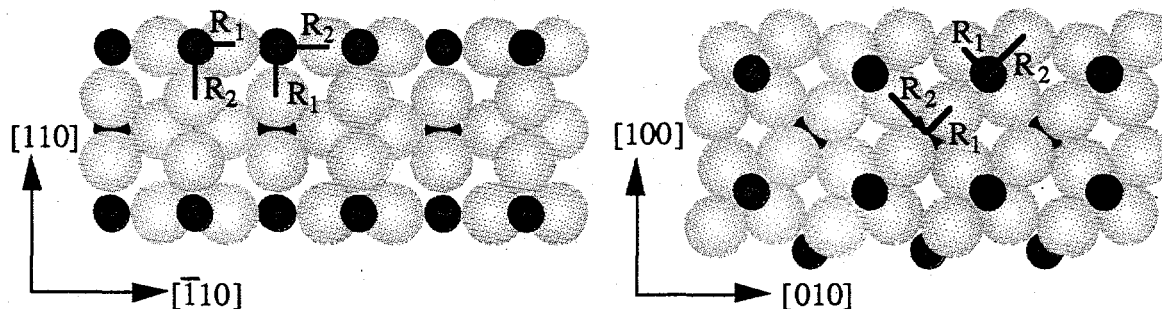


Fig. 7 Side views of  $TiO_2(110)$  (left) and (100) (right) lattices showing the orientations of the axial ( $R_2$ ) and equatorial ( $R_1$ ) bond lengths relative to the growth planes.

### Electronic Structure of $Nb_xTi_{1-x}O_2$

Having established the geometric structure of  $(Nb,Ti)O_2$  mixed rutiles, it is of interest to determine the electronic structure. We have done so with a combination of XPS and UPS valence band measurements. When present at the parts-per-thousand level, substitutional Nb creates a shallow donor level in the forbidden gap, making the material an n-type semiconductor. It is expected that this impurity state will evolve into a Nb-derived band which will overlap the conduction band as the amount of Nb increases, making the material metallic. However, the material was observed to remain transparent and insulating as more Nb was added. Valence band measurements reveal that the new occupied state density introduced by the addition of one electron per substitutional Nb does not develop near the conduction band, but rather in the valence band region. We show in figure 8 valence band measurements at normal emission excited with  $MgK\alpha$  x-rays (1253.6 eV) and He I ultraviolet radiation (21.2 eV) as a function of  $x$  for growth along (110). The new occupied state density starts  $\sim 4-5$  eV below the conduction band minimum (CBM) and extends to  $\sim 10$  eV below the CBM. There is some new state density seen  $\sim 1$  eV below the CBM in the He I excited spectra for  $x=0.10$ , but this feature was due to oxygen vacancy defects in the film created by growing under slightly oxygen poor conditions.

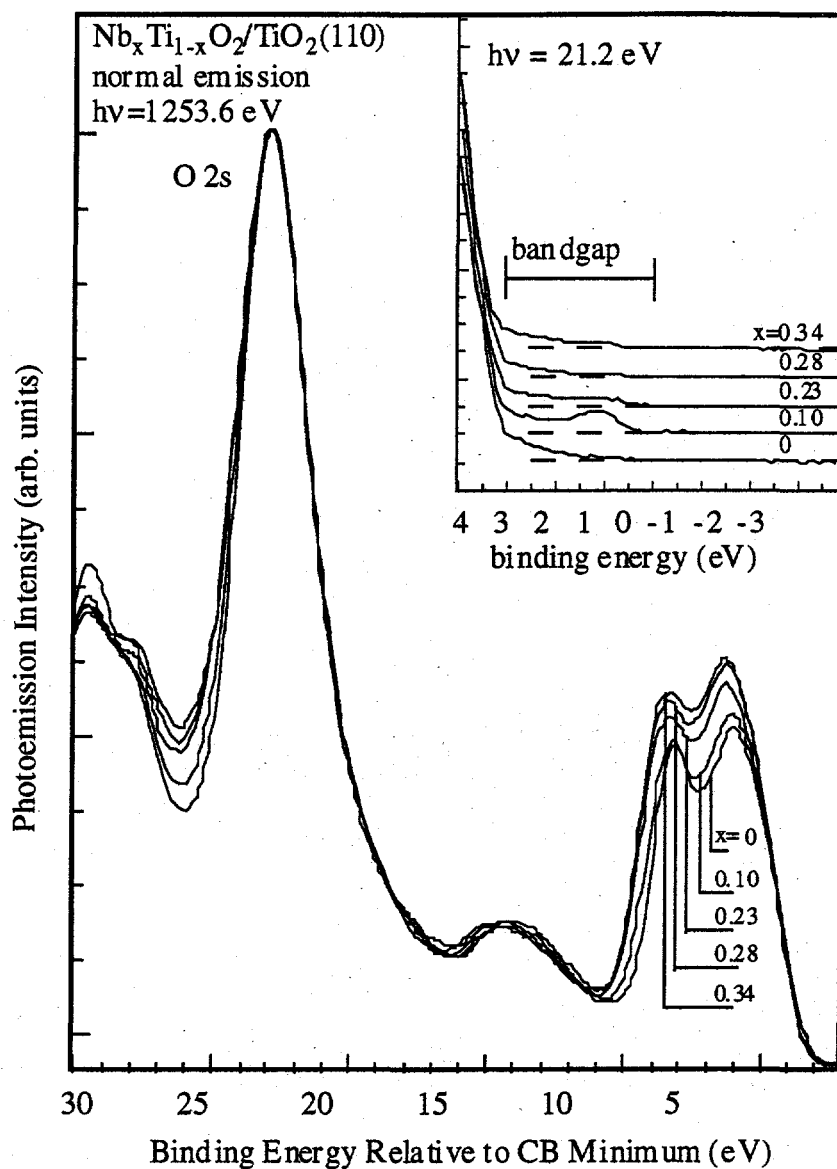


Fig. 8 Valence band spectra for epitaxial  $Nb_xTi_{1-x}O_2/TiO_2(110)$  as a function of  $x$ .

This experiment was done to see if the  $Nb_{0.1}Ti_{0.9}O_2$  films could be made conductive by creating a low concentration of oxygen vacancies. A control experiment in which growth was carried out under oxygen-rich conditions showed no new state density anywhere in the gap at  $x=0.10$  relative to that for pure  $TiO_2$ .

The substantial movement of the Nb-derived impurity level from an energy close to the conduction band minimum at the parts-per-thousand level to well within the valence band for Nb concentrations of at least several at. % raises interesting questions about the nature of this state. To appreciate these questions more fully, it is useful to consider the electron counting rule for compound semiconductors and insulators [17, 18]. This rule states that the number of electrons donated by each kind of atom in a particular bond is such that the bond will have a total of two electrons. In  $TiO_2$ , each Ti ion donates four valence electrons to each of six ionic bonds, or 0.67 electron per bond. Similarly, each O anion donates four valence electrons to each of three ionic bonds, or 1.33 electron per bond. Thus, there are 2.00 electrons per bond. On the (110) surface, the coordination of each bridging oxygen and each "exposed" Ti is reduced by one relative to the bulk. This reduced coordination produces a dangling bond at each exposed cation and bridging

oxygen site. There is nominally 0.67 electron per dangling cation bond, but the principle of autocompensation requires that this charge be transferred to the bridging oxygen dangling bond state. Since bridging oxygens and exposed Ti cations are present in a 1:1 ratio on the surface, all bridging oxygen dangling bonds are completely filled and all exposed cation dangling bonds are completely empty.

When Nb substitutes for Ti to form  $\text{Nb}_x\text{Ti}_{1-x}\text{O}_2$ , the  $3d^24s^2$  electrons which would normally be donated by Ti to the O 2p-derived valence band are replaced by four of the five electrons from the  $4d^45s^1$  Nb free-atom electron configuration. To first approximation, the valence band character is not expected to change with Nb substitution due to its largely O-2p character. The central question is - what happens to the extra Nb valence electron? Based on the electron counting rule, this electron cannot go into bonding states in the valence band, since each bond in the valence band already possesses a full complement of two electrons. Therefore, based on the electron counting rule, these extra electrons are expected to form a Nb-derived nonbonding band. Similarly, on the surface, the extra valence electron per Nb ion cannot transfer to bridging oxygen dangling bonds, because the latter are completely filled. Therefore, these electrons remain localized in Nb dangling bond states. The data presented in figure 8, together with the fact that these materials are insulators, make it clear that the new Nb-derived states are degenerate with the valence band. However, compliance with the electron counting rule precludes these states from being bonding in nature. Therefore, we conclude that these electrons are in localized, Nb-derived nonbonding states.

## DISCUSSION

The electronic structure model presented above has interesting implications for small-molecule chemisorption on  $\text{Nb}_x\text{Ti}_{1-x}\text{O}_2(110)$ . CO is amphoteric toward metals in a Lewis acid/base sense, and can adsorb by either electron donation from the CO- $\sigma$  orbital to the metal, or via back donation of metal d electrons to unoccupied CO- $\pi^*$  molecular orbitals. In interacting with oxides, CO may act as a Lewis acid, provided the cation has some available d electrons to donate to the  $\pi^*$  molecular orbital. However, CO does not adsorb on  $\text{TiO}_2(110)$  at temperatures as low as 110K, presumably due to the lack of available d electrons at Ti cation sites. However, CO adsorption at 110K may occur on  $\text{Nb}_x\text{Ti}_{1-x}\text{O}_2$  because of the availability of the nonbonding Nb electrons, which may increase the Lewis basicity of Nb cation sites. In contrast, Lewis bases such as  $\text{H}_2\text{O}$  should not bind any more strongly to Nb cation sites on  $\text{Nb}_x\text{Ti}_{1-x}\text{O}_2(110)$  than to Ti cation sites on pure  $\text{TiO}_2(110)$ . Preliminary experiments indicate that these two predictions are accurate, although more extensive experiments are planned for the near future.

The additional state density in the valence band region brought about by the formation of a Nb-derived, nonbonding band which is degenerate with the valence band is not sufficient to account for the factor-of-two increase in extent of photochemical destruction of dichlorobenzene (DCB) [2]. The effect was seen for only a few atomic percent addition of  $\text{Nb}_2\text{O}_5$  to  $\text{TiO}_2$ , and actually decreases with the addition of more  $\text{Nb}_2\text{O}_5$ . Higher state density 4 to 10 eV below the conduction band minimum is observed by electron energy loss spectroscopy to give rise to increased dipole oscillator strength for transition energies of 4 to 8 eV, but this increase is not as great as that observed in the extent of DCB destruction [2]. Thus, we tentatively conclude that in addition to adding oscillator strength in the ultraviolet, which would increase the rate of electron-hole pair excitation, substitutional Nb in the lattice also decreases the recombination velocity. The combined effect of higher electron-hole pair production rate and longer lifetimes may explain the 100% increase in extent of DCB destruction. However, more work is needed to further elucidate this mechanism.

Finally, substitutional Nb in  $\text{TiO}_2$  has been found to reduce the extent of interfacial reaction with thin films of Pt metal to almost zero compared to the case of pure  $\text{TiO}_2$ . These reactions give rise to the strong-metal support interaction (SMSI) effect, which poisons metal catalysts which are supported by oxide particles [19]. In this effect, interfacial reaction between the metal and the oxide gives rise to suboxide formation and subsequent diffusion over the surface of the metal. The presence of a thin suboxide film on the catalyst surface poisons the latter. Based on

the relative extents of reaction of Pt with bulk reduced and fully stoichiometric  $\text{TiO}_2$ , we have proposed that oxygen vacancy migration from the bulk to the surface (or, equivalently, oxygen migration from the surface to the bulk) through interdiffusion is a major driver in the formation of suboxides at the Pt/ $\text{TiO}_2$  interface [20]. The tendency of Nb-doping to further impede suboxide formation may come about because of lower oxygen vacancy diffusion coefficients in  $\text{Nb}_x\text{Ti}_{1-x}\text{O}_2$  compared to those in pure  $\text{TiO}_2$ . The fact that the vacuum annealing process which makes  $\text{TiO}_2$  sufficiently semiconducting to do STM leaves  $\text{Nb}_x\text{Ti}_{1-x}\text{O}_2/\text{TiO}_2(100)$  in an insulating state supports this hypothesis. Indeed, we have found that it is exceedingly difficult to bulk reduce  $\text{Nb}_x\text{Ti}_{1-x}\text{O}_2/\text{TiO}_2$  specimens by annealing in vacuum. The inability of oxygen vacancies to diffuse to the surface would make the interface more inert with respect to  $\text{TiO}_x$  suboxide formation, which is what we observe.

## CONCLUSIONS

We have explored the synthesis of model, single-crystal phases of  $\text{Nb}_x\text{Ti}_{1-x}\text{O}_2$  by MBE for the purpose of definitive surface thermal- and photochemical research on mixed-metal oxides. We have found that it is possible to selectively modify the electronic structure of the oxide without changing its geometric structure by adding Nb up to the point that misfit dislocations form. This concentration is as high as 30 at. % in the (110) orientation. The addition of Nb to the lattice at concentrations below the onset of dislocation formation produces strained but virtually defect free rutile with the same lattice parameters as  $\text{TiO}_2$  (to within  $\sim 0.1\text{\AA}$ ), and a new Nb-derived nonbonding band which is degenerate with the valence band. The modified electronic structure changes the extent and nature of surface chemistry with small molecules and metal overlayers, as well as the photochemical activity of the surface with respect to the destruction of chlorinated organics.

## ACKNOWLEDGMENTS

The authors gratefully acknowledge partial support from the US Department of Energy, Office of Basic Energy Sciences, Materials Science Division under Contracts DE-AC06-76RLO 1830 (PNNL) and W-31-109-ENG-38 (ANL). The ion channeling analysis at Montana State University was supported in part by NSF Grant DMR 9409205.

## REFERENCES

- [1] A. Mills, R. H. Davies and D. Worsley, *Chem. Soc. Rev.*, 417 (1993).
- [2] H. Cui, K. Dwight, S. Soled and A. Wold, *J. Solid State Chem.* **115**, 187 (1995).
- [3] S. A. Chambers, T. T. Tran and T. A. Hileman, *J. Mat. Res.* **9**, 2944 (1994).
- [4] Y. Gao, Y. Liang and S. A. Chambers, *Surf. Sci.* **348**, 17 (1996).
- [5] Y. Gao and S. A. Chambers, *J. Mater. Res.* **11**, 1025 (1996).
- [6] S. A. Chambers, Y. Gao, S. Thevuthasan, Y. Liang, N. R. Shivaparan and R. J. Smith, *J. Vac. Sci. Technol.* to appear, (1996).
- [7] P. Zschack, J. B. Cohen and Y. W. Chung, *Surface Sci.* **262**, 395 (1992).
- [8] P. W. Murray, F. M. Leibsle, H. J. Fisher, C. F. J. Flipse, C. A. Muryn and G. Thornton, *Phys. Rev. B* **46**, 12877 (1992).
- [9] P. W. Murray, F. M. Leibsle, C. A. Muryn, H. J. Fisher, C. F. J. Flipse and G. Thornton, *Phys. Rev. Lett.* **72**, 689 (1994).

- [10] P. W. Murray, F. M. Leibsle, C. A. Muryn, H. J. Fisher, C. F. J. Flipse and G. Thornton, *Surf. Sci.* **321**, 217 (1994).
- [11] P. J. Hardman, N. S. Prakash, C. A. Muryn, G. N. Raikar, A. G. Thomas, A. F. Prime, G. Thornton and R. J. Blake, *Phys. Rev. B* **47**, 16056 (1993).
- [12] B. G. Hyde and S. Andersson, *Inorganic Crystal Structures*, (John Wiley & Sons, New York, 1989).
- [13] R. W. G. Wyckoff, *Crystal Structures*, (John Wiley & Sons, New York, 1963), 1.
- [14] S. A. Chambers, *Adv. in Phys.* **40**, 357 (1991).
- [15] S. A. Chambers, Y. Gao, Y. J. Kim, M. A. Henderson, S. Thevuthasan, S. Wen and K. L. Merkle, *Surf. Sci.*, to appear (1996).
- [16] S. Thevuthasan, N. Shivaparan, R. J. Smith, Y. Gao and S. A. Chambers, unpublished.
- [17] J. P. LaFemina, *Crit. Rev. Surf. Chem.* **3**, 297 (1994).
- [18] M. D. Pashley, *Phys. Rev. B* **40**, 10481 (1989).
- [19] S. J. Tauster, S. C. Fung and R. L. Garten, *J. Amer. Chem. Soc.* **100**, 170 (1978).
- [20] Y. Gao, Y. Liang and S. A. Chambers, *Surf. Sci.*, to appear, (1996).

---

#### DISCLAIMER

This report was prepared as an account of work sponsored by an agency of the United States Government. Neither the United States Government nor any agency thereof, nor any of their employees, makes any warranty, express or implied, or assumes any legal liability or responsibility for the accuracy, completeness, or usefulness of any information, apparatus, product, or process disclosed, or represents that its use would not infringe privately owned rights. Reference herein to any specific commercial product, process, or service by trade name, trademark, manufacturer, or otherwise does not necessarily constitute or imply its endorsement, recommendation, or favoring by the United States Government or any agency thereof. The views and opinions of authors expressed herein do not necessarily state or reflect those of the United States Government or any agency thereof.